Coherence measurements with the two-photon Michelson interferometer

Dorilian Lopez-Mago[1,2] and Lukas Novotny[1]

[1]*Institute of Optics, University of Rochester, Rochester, New York 14627, USA*
[2]*Photonics and Mathematical Optics Group, Tecnológico de Monterrey, Monterrey 64849, Mexico*

The interference of entangled photon pairs permits the study of the fundamental properties of quantum mechanics. The process is also finding practical applications in optical imaging. The Michelson interferometer provides an elegant means for characterizing the degree of two-photon entanglement, but the technique has not yet been described and analyzed in detail. Here we provide a full description of the interference of collinear down-converted photons in a Michelson interferometer. We explain the basic elements that characterize the interference pattern and complement the theory with experimental measurements. The two-photon Michelson interferometer can be used in quantum optical coherence tomography for dispersion-free imaging and localization.

I. INTRODUCTION

The seminal paper of Einstein, Podolsky, and Rosen (EPR) analyzes a thought experiment that is based on the combined quantum state of two spatially separate systems [1]. Two particles with known quantum states interact for a period of time and then separate. After the interaction, it is no longer possible to determine the quantum state of each particle separately. According to quantum mechanics, the combined system of particles I + II has become entangled. The measurement of one particle instantly modifies the state of the second particle, even if the two particles are spatially separated. The EPR paper criticizes this interpretation of quantum mechanics and argues that the theory is incomplete. The missing parameters are known as hidden variables. Entanglement remained a philosophical topic until the paper of J. S. Bell [2], who showed that by performing correlation experiments, one is capable of testing the predictions of quantum mechanics and of hidden-variable theories. Bell's correlation measurements have been tested [3–5] and the results agree with the description of quantum mechanics.

Photons are particularly attractive for studying the implications of entanglement since the generation of correlated photons is possible with the process of spontaneous parametric down-conversion (SPDC) [6,7]. This nonlinear process produces pairs of photons that are correlated in time, energy, and momentum. SPDC was first predicted to be a background noise term in the process of parametric amplification and has been termed "parametric luminescence" [8]. The statistical properties of SPDC were studied by Zel'dovich *et al.* [6] and experimentally measured by Burnham *et al.* [7]. Photons generated by SPDC cannot be explained by two independent sources and their correlation is intimately related by the energy uncertainty and emission time.

The properties of down-converted photons can be understood on the basis of energy and momentum conservation. A single photon, called the pump, propagating in a nonlinear crystal can spontaneously split into two photons, called signal and idler. Energy conservation implies that the frequencies of the photons satisfy $\omega_p = \omega_s + \omega_i$, where p, s, and i refer to pump, signal, and idler, respectively. The direction of the photons is determined by momentum conservation, $\mathbf{k}_p = \mathbf{k}_s + \mathbf{k}_i$. After the work of Burnham *et al.* [7], SPDC

has been used in various experiments for the generation of entangled photon pairs. Entanglement in various degrees of freedom has been demonstrated, for example, in polarization [9,10], energy [11], and momentum [12].

The interference of down-converted photons was thoroughly studied by Mandel and collaborators [13]. Traditional interference measurements typically employ a single-photon detector to measure the probability of detecting a photon as a function of the phase difference between the interferometer arms. Interference occurs because the two optical paths are indistinguishable, meaning that the experiment cannot distinguish which path was chosen by the photon. On the other hand, two-photon interference detects photon pairs and measures the probability of simultaneously detecting two photons with a pair of photodetectors. The probability of detecting coincidences depends on the phase difference in the two interferometer arms. Interference occurs due to the indistinguishability of the different ways the photon pairs can propagate through the interferometer. Two-photon interference with photon pairs generated by SPDC has become a standard tool for studying the quantum properties of light [13].

Two-photon interference with down-converted photons has evolved into several applications [14–16]. In particular, quantum optical coherence tomography (QOCT) uses frequency-entangled photons in a Hong-Ou-Mandel [17] interferometer in order to generate depth resolution in the imaging of a sample positioned in one of the interferometer arms. QOCT improves depth resolution by a factor of two compared with its classical counterpart. In addition, QOCT is immune to dispersion effects because of photon entanglement.

In recent decades, several experiments have been undertaken to demonstrate fourth-order interference effects using entangled down-converted photons [10,11,17–22]. Most of these studies concentrate on the nonlocal nature of entanglement and the violation of Bell inequalities. These experiments rely on a spatial separation of entangled photons pairs, i.e., the down-converted photons are *not* collinear. For example, the Franson experiment [11,23] uses two separate interferometers to observe the violation of a Bell inequality in position and time. Another example is the demonstration of entangled photon bunching with a Hong-Ou-Mandel interferometer [17], where two noncollinear down-converted photons enter

separate input ports of a beam splitter. However, there are only a few fourth-order interference experiments that use *collinear* down-converted photons. In the collinear geometry, down-converted photon pairs become spatially indistinguishable.

Galvez *et al.* and Odate *et al.* have recently measured collinear fourth-order interference [24,25], but these studies did not consider the spectral properties of the pump photons. Furthermore, the measurements have been performed for restricted path-length differences. In the present study, we account for the spectral density of the pump and record a *complete* fourth-order interferogram. We show that the interferogram is significantly influenced by the coherence properties of the pump laser and we derive an equation that accounts for the pump's spectral density. A quantitative comparison of theory and experiment is presented.

In order to realize a test of Bell's inequality, we require spatially separated, down-converted photons. For the collinear case, the degree of photon-pair entanglement is determined by the ratio of the emission bandwidth to the pump bandwidth. Our measurements show that the fourth-order interferogram is influenced by the degree of entanglement in a controllable and predictive manner. Our experiments make use of a two-photon Michelson interferometer, but similar results could be obtained using a Mach-Zehnder interferometer, which is equivalent to selecting a different output port.

This paper is organized as follows: Sec. II introduces basic concepts and presents a derivation of the joint spectral density of down-converted photons pairs. Section III analyzes the interference pattern recorded with a two-photon Michelson interferometer. Section IV presents experimental data and a comparison with theory. Finally, in Sec. V, we provide a discussion that includes possible applications.

II. THE JOINT SPECTRAL DENSITY OF ENTANGLED DOWN-CONVERTED PHOTONS

Let us start with a single-photon wave-packet state, written as a weighted superposition of monochromatic modes [26],

$$|1\rangle = \int d\omega \, \phi(\omega)|\omega\rangle, \tag{1}$$

with $\phi(\omega)$ being the probability amplitude of state $|\omega\rangle$. For the purpose of this paper, we consider linear polarization and propagation in one dimension. A monochromatic mode $|\omega\rangle$ is the ket representation of a monochromatic plane wave with frequency ω. The monochromatic modes satisfy the orthogonality condition $\langle\omega'|\omega\rangle = \delta(\omega' - \omega)$, which ensures that $\langle\omega'|1\rangle = \phi(\omega')$. According to the interpretation of quantum mechanics, $|\langle\omega'|1\rangle|^2 = |\phi(\omega')|^2$ is the probability that when the photon is detected, $|1\rangle$ *collapses* into the state $|\omega'\rangle$. The function $\Phi(\omega) = |\phi(\omega)|^2$ is the spectral density, which is equivalent to the frequency spectrum. $\Phi(\omega)$ is normalized $[\int \Phi(\omega)d\omega = 1]$ and has a center frequency $\overline{\omega}$ and bandwidth $\Delta\omega$.

A photodetector measures photon absorption without distinguishing between different frequency components. Therefore, the probability P_1 of detecting a single-photon state is equivalent to $P_1 = \int d\omega' |\langle\omega'|1\rangle|^2$, where the integration is over the monochromatic modes that enter the detector. For example, consider that the detector records all of the monochromatic

modes of the state given in Eq. (1). Then, the probability of detecting that photon is $\int d\omega' \Phi(\omega') = 1$. However, if we spatially separate the monochromatic modes (e.g., using a prism) and project them in a photodetector array, then only one cell of the array will respond. The probability of responding will be given by $\Phi(\omega')\,d\omega'$.

Let us now consider the detection of two photons. The quantum state $|1,1\rangle$ of a pair of photons is given by the joint state $|1,1\rangle = |1\rangle \bigotimes |1\rangle$. This state is more subtle than the single-photon state defined in Eq. (1). If the detection of one photon does not alter the state of the second photon, then the two photons are independent and the joint state is separable. But, if the detection of one photon affects the state of the second photon, then $|1,1\rangle$ is entangled. The joint state of two photons can be written as

$$|1,1\rangle = \iint d\omega_1 d\omega_2 \, \phi(\omega_1,\omega_2)|\omega_1\rangle|\omega_2\rangle. \tag{2}$$

For the following, we assume that the monochromatic modes have the same polarization and propagation direction. The joint spectral density $\Phi(\omega_1,\omega_2) = |\phi(\omega_1,\omega_2)|^2$ is the probability of detecting one photon with frequency ω_1 and a second photon with frequency ω_2. The joint spectral density is normalized, $\int d\omega_1 d\omega_2 \Phi(\omega_1,\omega_2) = 1$. If $\phi(\omega_1,\omega_2)$ can be factored into separate functions of ω_1 and ω_2, then the state $|1,1\rangle$ is separable, otherwise it is entangled.

A separable state can be expressed as the product of two photons, $|1,1\rangle = |1(\omega_1)\rangle|1(\omega_2)\rangle$, where $|1(\omega_i)\rangle = \int d\omega_i \phi(\omega_i)|\omega_i\rangle$ $(i = 1,2)$. The joint spectral density becomes $\Phi(\omega_1,\omega_2) = \Phi_1(\omega_1)\Phi_2(\omega_2)$. If each photon is symmetric with respect to a center angular frequency ω_0, then the joint spectral density of a separable state is symmetric in the plane (ω_1,ω_2) with respect to $(\omega_1,\omega_2) = (\omega_0,\omega_0)$, as shown in Fig. 1(a). On the contrary, $\Phi(\omega_1,\omega_2)$ is asymmetric for an entangled state and depends on the correlation between both photons. For example, Fig. 1(b) shows the joint spectral density of an anticorrelated entangled state. Note that an entangled state is a state which cannot be factored in any basis [27] and that the entangled state defined by Eq. (2) is denoted a time-energy entangled state.
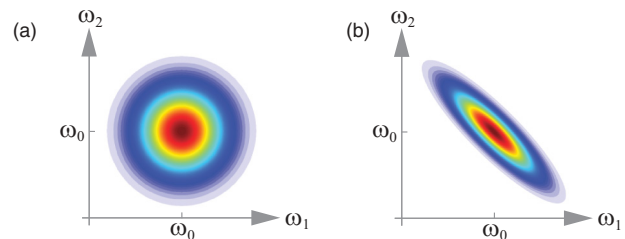

FIG. 1. (Color online) The joint spectral density $\Phi(\omega_1,\omega_2) = |\phi(\omega_1,\omega_2)|^2$ of a two-photon state, $|1,1\rangle = \iint d\omega_1 d\omega_2 \, \phi(\omega_1,\omega_2)|\omega_1,\omega_2\rangle$, can be either (a) separable or (b) entangled. ω_0 is the center angular frequency of each photon. If the state is separable, then $\Phi(\omega_1,\omega_2)$ is symmetric in the plane (ω_1,ω_2), centered at ω_0, and the state $|1,1\rangle$ can be factored as the product of two photons, $|1,1\rangle = |1(\omega_1)\rangle|1(\omega_2)\rangle$. If the two photons are in an energy-entangled state, then $|1,1\rangle$ cannot be factored and the joint spectral density is asymmetric in the plane (ω_1,ω_2).

Typical photodetectors cannot resolve the number of photons received. Therefore, two-photon states are measured using correlations between two separate photodetector signals. The probability of detecting a two-photon state is $P_{1,2} = \iint d\omega_1' d\omega_2' |\langle \omega_1', \omega_2' | 1, 1 \rangle|^2$.

A. The quantum state of down-converted photons

A widely used method for generating energy-entangled photons is spontaneous parametric down-conversion (SPDC). In this nonlinear process, a pump photon is spontaneously split into two photons. The daughter photons are traditionally called signal and idler. SPDC takes place inside a nonlinear crystal with a $\chi^{(2)}$ nonlinearity. Energy and momentum conservation imply $\hbar\omega_p = \hbar\omega_s + \hbar\omega_i$ and $\hbar\mathbf{k}_p = \hbar\mathbf{k}_s + \hbar\mathbf{k}_i$, respectively, where $\hbar\omega_j$ and $\hbar\mathbf{k}_j (j = p, s, i)$ are the energies and momenta of the pump (p), signal (s), and idler (i) photons. Due to the fact that there are many ways to partition the energy of the pump photon, the signal and idler photons have a broad spectral density. SPDC produces energy-entangled states of the form $|1, 1\rangle = \int_0^{\omega_p} d\omega \, \phi(\omega) |\omega\rangle |\omega_p - \omega\rangle$, where ω_p is the energy of the pump photon and $|\phi(\omega)|^2$ is the joint spectral density. Clearly, the state cannot be factored and the two photons are entangled. It is also possible to prepare the photons in a momentum-entangled state by filtering the emission directions of the down-converted photons, or in a polarization-entangled state. It is even possible to create hyperentangled states [27].

The SPDC process is commonly classified according to the polarization of the down-converted photons. In type-I SPDC, signal and idler photons have polarization directions orthogonal to the pump polarization. In type-II SPDC, the polarization of signal and idler photons are orthogonal, with one of them having the same polarization as the pump. If the center frequencies of signal and idler are the same, $\overline{\omega}_s = \overline{\omega}_i = \omega_0$, then one speaks of degenerate down-conversion. In the case when the down-converted photon pairs propagate collinearly, the photons must be degenerate. For the purpose of this paper, we consider type-I, collinear, down-converted photons with degenerate center angular frequency $\omega_0 = \overline{\omega}_p/2$, where $\overline{\omega}_p$ is the center angular frequency of the pump laser.

The joint spectral density $\Phi(\omega_s, \omega_i) = |\phi(\omega_s, \omega_i)|^2$ of the down-converted photons depends on the pump spectral density $P(\omega_p) = |p(\omega_p)|^2$ and the physical properties of the nonlinear crystal. In what follows, $P(\omega_p)$ has a bandwidth $\Delta\omega_p$ (FWHM) and center angular frequency $\overline{\omega}_p$. $\phi(\omega_s, \omega_i)$ has been

calculated by Ou [28] as

$$\phi(\omega_s, \omega_i) = \int d\omega_p \, p(\omega_p) h(\omega_s, \omega_i, \omega_p) \delta(\omega_s + \omega_i - \omega_p), \quad (3)$$

$$h(\omega_s, \omega_i, \omega_p) = \mathrm{sinc}(\Delta K L/2), \quad (4)$$

with $h(\omega_s, \omega_i, \omega_p)$ being the phase-matching function and $\Delta K = [n_e(\omega_p)\omega_p - n_o(\omega_s)\omega_s - n_o(\omega_i)\omega_i]/c$ being the phase-matching condition; and for a uniaxial crystal with extraordinary and ordinary index of refraction, n_e and n_o, respectively, L is the length of the crystal. The $\delta(\omega_s + \omega_i - \omega_p)$ is associated with the conservation of energy.

We proceed to discuss the characteristics of the joint spectral density. After integrating over the δ function in Eq. (3), we obtain

$$\Phi(\omega_s, \omega_i) = P(\omega_s + \omega_i)H(\omega_s, \omega_i). \quad (5)$$

The function $H(\omega_s, \omega_i) = |h(\omega_s, \omega_i, \omega_s + \omega_i)|^2$ corresponds to a bandpass function with bandwidth $\Delta\omega_H$ and center angular frequency $\overline{\omega}_H = \overline{\omega}_p/2$. The bandwidth $\Delta\omega_H$ depends on the group-velocity dispersion $k_o'' = d^2 k_o/d\omega^2|_{\omega=\omega_0}$, where $k_o = n_o(\omega)\omega/c$, by the relation $\Delta\omega_H = 2\sqrt{2\pi/L|k_o''|}$. Typically, $\Delta\omega_H$ is of the order of $10^{12\sim13}$ Hz. In general, for a cw pump laser, $\Delta\omega_H > \Delta\omega_p$. As mentioned before, an entangled two-photon state corresponds to an asymmetric joint spectral density. We will show that the degree of entanglement is proportional to $\gamma = \Delta\omega_H/\Delta\omega_p$. However, γ is only a relative value that can be used for comparison between experiments. For example, compared to a pulsed laser, the degree of entanglement generated by a cw laser is higher since $\Delta\omega_p^{(\mathrm{Pulsed})} > \Delta\omega_p^{(\mathrm{cw})}$ and hence $\gamma^{(\mathrm{Pulsed})} < \gamma^{(\mathrm{cw})}$. Unfortunately, a more robust parameter of the degree of entanglement (e.g., a Bell's inequality) cannot be realized with collinear entangled photons (we need two spatially separated interferometers [11]). Still, since the interference pattern depends on $\Phi(\omega_s, \omega_i)$, we can infer from the interferogram whether the joint spectral density is separable or entangled.

Figure 2 shows the joint spectral density of type-I down-converted photons for a cw pump laser. We consider that the spectrum of the pump photons $P(\omega_p)$ is Gaussian. The bandwidth of $P(\omega_p)$ controls the width of the joint spectral density along $\omega_s = \omega_i$. For a narrow pump bandwidth, the spectrum is concentrated along the line $\omega_s + \omega_i = \overline{\omega}_p$; on the other hand, for a large pump bandwidth (e.g., a pulsed laser), the spectrum is smeared out in the plane (ω_1, ω_2) and the degree of entanglement is considerably reduced, since $\gamma \to 0$ as $\Delta\omega_p$ is increased.
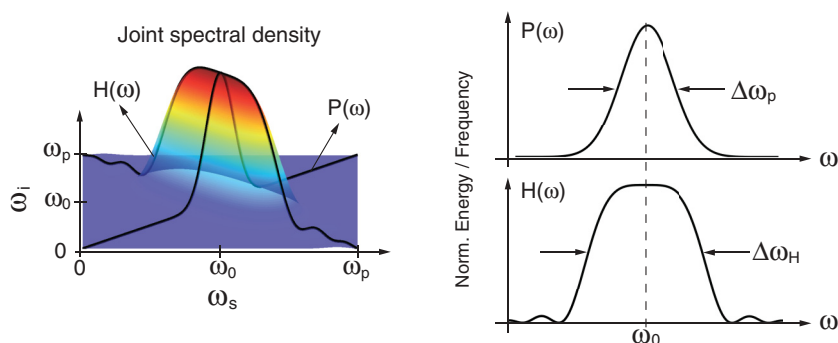

FIG. 2. (Color online) The joint spectral density of type-I down-converted photons, $\Phi(\omega_s, \omega_i) = P(\omega_s + \omega_i)H(\omega_s, \omega_i)$, depends on the spectral density $P(\omega_p)$ of the pump photons and the phase-matching function $H(\omega_s, \omega_i)$ of the crystal. The degree of entanglement is proportional to the ratio $\gamma = \Delta\omega_H/\Delta\omega_p$, where $\Delta\omega_p$ and $\Delta\omega_H$ are the bandwidths of the pump laser and the phase-matching function, respectively.

The detection of photon pairs is accomplished by two photodetectors working in coincidence. Bandpass filters can be introduced in the light path either after the crystal or in front of the photodetectors. The filters modify the joint spectral density as

$$\Phi(\omega_s, \omega_i) \rightarrow F_s(\omega_s) F_i(\omega_i) \Phi(\omega_s, \omega_i), \qquad (6)$$

where F_s and F_i are the spectral transmissivities of the filters in detection paths s and i, respectively. We will assume that the bandpass filters have the following normalized spectral transmissivity:

$$F(\omega) = \begin{cases} 1/\Delta\omega_F & |\omega - \overline{\omega}_F| < \Delta\omega_F/2 \\ 0 & |\omega - \overline{\omega}_F| > \Delta\omega_F/2, \end{cases} \qquad (7)$$

where $\overline{\omega}_F$ is the central frequency and $\Delta\omega_F$ is the bandwidth. The bandpass filters select a frequency region in the (ω_s, ω_i) plane. Therefore, the quantum state and the factor γ are modified after the filters. To avoid reducing the degree of entanglement, it is favorable that the bandwidth of the filters satisfies $\Delta\omega_F > \Delta\omega_p$.

Let us now rewrite the two-photon state by substituting Eq. (3) into Eq. (2), but instead of integrating over ω_p, we integrate over ω_i,

$$|1, 1\rangle = \iint d\omega_s d\omega_p \phi(\omega_s, \omega_p - \omega_s)|\omega_s\rangle|\omega_p - \omega_s\rangle. \qquad (8)$$

We have used $\phi(\omega_s, \omega_p - \omega_s) = p(\omega_p) h(\omega_s, \omega_p - \omega_s, \omega_p)$. In this form, the pump spectral density depends on a single variable. Furthermore, since $\Delta\omega_H > \Delta\omega_p$ for a cw laser, we can assume that $H \approx 1$ in the spectral region defined by the filters. We further assume that the filters are identical and that their central frequency is $\overline{\omega}_F \approx \omega_0$. Furthermore, the filter bandwidth is larger than the linewidth of the pump laser, which yields $\Delta\omega_p < \Delta\omega_F < \Delta\omega_H$. Making use of the symmetry of the bandpass filters, $F(\omega_s) = F(\omega_p - \omega_s)$ and $F(\omega) \propto F^2(\omega)$, allows us to write the joint spectral density in the compact form

$$\Phi(\omega_s, \omega_p - \omega_s) \approx P(\omega_p) F(\omega_s). \qquad (9)$$

Thus, the joint spectral density and hence the degree of entanglement can be controlled with two experimental parameters: the bandwidth of the pump laser and the bandwidth of the filters.

III. ANALYSIS OF THE TWO-PHOTON MICHELSON INTERFEROMETER

As illustrated in Fig. 3, we will compare the operating principles of the one-photon and the two-photon Michelson interferometer [13]. In the former, a single photon enters the interferometer and a single photodetector D1 measures the probability $P_1(\tau)$ of detecting the photon as a function of the time difference $\tau = t_2 - t_1$ (or path-length difference x) defined by the arm lengths of the interferometer. Because the interference pattern or interferogram depends on the second power of the optical field, we refer to $P_1(\tau)$ as the second-order interferogram. In the two-photon Michelson interferometer, photon pairs enter the interferometer and two photodetectors working in coincidence are used to measure the joint probability $P_{1,2}(\tau)$ of detecting one photon at D1 and one
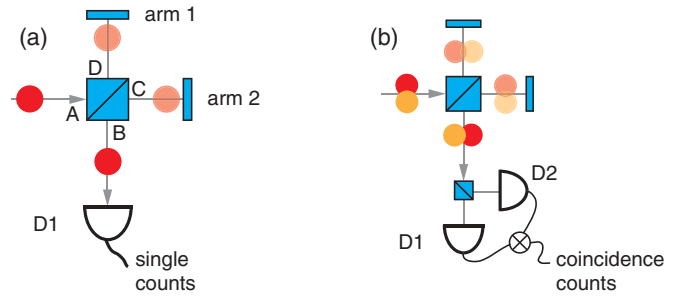

FIG. 3. (Color online) Illustration of one-photon and two-photon Michelson interferometers. (a) In a one-photon Michelson interferometer, one photodetector measures the probability of detecting a single photon as a function of the time difference τ defined by the path-length difference x of the interferometer arms. (b) In a two-photon Michelson interferometer, two photodetectors working in coincidence are used to measure the simultaneous arrival of photon pairs as a function of time delay τ.

photon at D2. $P_{1,2}(\tau)$ is called the fourth-order interferogram because it depends on the fourth power of the optical field.

Interference can be viewed as the consequence of the indistinguishability of possible experimental outcomes. In the one-photon Michelson interferometer, a photon can "choose" between two paths to travel through the interferometer [Fig. 4(a)]. If the experiment is not capable of determining which path is taken by the photon, then the two possibilities interfere. On the other hand, if it is possible to tell which path was taken, then there is no interference. In the latter case, the probability of the outcome is determined by the classical sum of probabilities.

In the two-photon Michelson interferometer, there are four possibilities for a pair of photons to travel through the interferometer. Both photons can be transmitted, both can be reflected, or one can be transmitted or reflected while the other is reflected or transmitted [Fig. 4(b)]. The indistinguishability of the four possibilities produces interference in the coincidence counts. However, the photons do not interfere with each other; the pair of photons interferes with the pair itself [13]. The interference pattern $P_{1,2}(\tau)$ depends on the correlation between
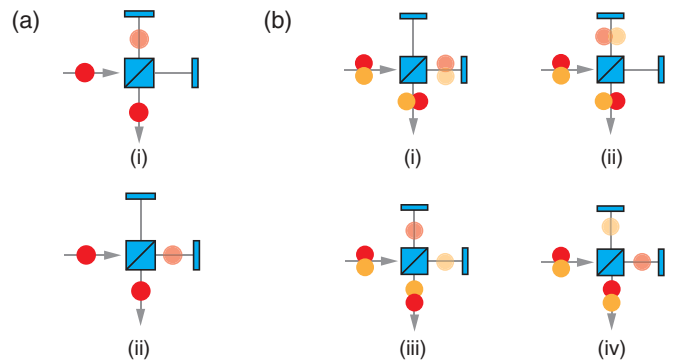

FIG. 4. (Color online) Interference of different photon paths in a (a) one-photon and (b) two-photon Michelson interferometer. In (a), a photon can travel along two different paths (i) and (ii). In (b), a pair of photons can travel along four different paths. Interference in coincidence counting occurs because of the indistinguishability of the different paths.

the two photons. If the two photons are independent, then $P_{1,2}(\tau)$ is the product of two second-order interferograms, $P_{1,2}(\tau) = P_1(\tau)P_2(\tau)$. On the other hand, if the photon pair is in an entangled state, then the interference pattern depends on the joint spectral density of the two-photon state. Thus the degree of entanglement γ can be extracted from the interferogram.

Let us review the one-photon Michelson interferometer from a quantum mechanical perspective. The quantum state of a single-photon wave packet is given by Eq. (1). A photon in state $|\omega\rangle$ enters the beam splitter through input port A [Fig. 3(a)] and after it passes through the beam splitter its state becomes [24]

$$|\omega\rangle = r|\omega\rangle_d + t|\omega\rangle_c, \qquad (10)$$

where d and c refer to the output ports D and C, respectively. The constants r and t are the reflection and transmission coefficients, respectively. $|\omega\rangle_d$ evolves along path 1 and acquires a phase $\exp(i\omega t_1)$. After exiting the beam splitter through output port B, it becomes $|\omega\rangle_d = t\exp(i\omega t_1)|\omega\rangle_b$. In the same way, $|\omega\rangle_c$ acquires a phase $\exp(i\omega t_2)$ and at the output port B becomes $|\omega\rangle_c = r\exp(i\omega t_2)|\omega\rangle_b$. By substituting $|\omega\rangle_d$ and $|\omega\rangle_c$ into Eq. (10), we obtain $|\omega\rangle = rt[\exp(i\omega t_1) + \exp(i\omega t_2)]|\omega\rangle_b$. The single-photon wave-packet state defined by Eq. (1) now becomes

$$|1\rangle \propto \int d\omega\, \phi(\omega)(1 + e^{i\omega\tau})|\omega\rangle, \qquad (11)$$

where $\tau = t_2 - t_1$. For simplicity, we discarded the label b. Using the fact that $\Phi(\omega) = |\phi(\omega)|^2$ is normalized and has a center angular frequency $\overline{\omega}$ allows us to calculate the second-order interferogram $P(\tau) = \int d\omega' |\langle\omega'|1\rangle|^2$ as

$$P(\tau) \propto 1 + \Gamma(\tau)\cos(\overline{\omega}\tau). \qquad (12)$$

The function $\Gamma(\tau) = \int d\omega' \Phi(\omega' + \overline{\omega})\cos(\omega'\tau)$ corresponds to the Fourier transform of the spectral density.

The interferogram features two contributions: a dc term and an interference term. The interference term produces oscillations (fringes) with frequency $\overline{\omega}$ and an amplitude modulation $\Gamma(\tau)$. Practically, we can relate τ to the path-length difference $x = 2(l_2 - l_1)$ through $\tau = x/c$, where l_1 and l_2 are the lengths of the interferometer arms and c is the speed of light. Γ defines the coherence length L_c through $\Gamma(L_c) = \frac{1}{2}\Gamma_{\max}$, that is, L_c is the half width at half maximum. L_c depends on the shape of $\Phi(\omega)$ and is related to a spectral bandwidth, $\Delta\omega \sim c/L_c$. Experimentally, $\Gamma(x)$ is referred to as the visibility,

$$V = \frac{I_{\max} - I_{\min}}{I_{\max} + I_{\min}}, \qquad (13)$$

with $I_{\max}$ and $I_{\min}$ being the maximum and minimum intensities of the fringes, respectively.

We now turn to the description of the two-photon Michelson interferometer. The beam splitter acts separately on each monochromatic state $|\omega_1\rangle$ and $|\omega_2\rangle$. Thus, we can use the previous result $|\omega\rangle \rightarrow rt[\exp(i\omega t_1) + \exp(i\omega t_2)]|\omega\rangle$ to obtain the transformed two-photon state defined in Eq. (2) as

$$|1,1\rangle \propto \iint d\omega_1 d\omega_2\, \phi(\omega_1,\omega_2)(1 + e^{i\omega_1\tau})(1 + e^{i\omega_2\tau})|\omega_1\rangle|\omega_2\rangle. \qquad (14)$$

The corresponding fourth-order interferogram is $P_{1,2}(\tau) = \iint d\omega_1' d\omega_2' |\langle\omega_1',\omega_2'|1,1\rangle|^2$. The second beam splitter does not affect the interference pattern; it only reduces the intensity of the coincidences by a factor of $1/2$. For the special case where $\phi(\omega_1,\omega_2)$ is separable, that is, $\Phi(\omega_1,\omega_2) = \Phi(\omega_1)\Phi(\omega_2)$, $P_{1,2}(\tau)$ can be written as the product of two second-order interferograms,

$$P_{1,2}(\tau) \propto [1 + \Gamma_1(\tau)\cos(\overline{\omega}_1\tau)][1 + \Gamma_2(\tau)\cos(\overline{\omega}_2\tau)], \qquad (15)$$

where $\Gamma_1(\tau)$ and $\Gamma_2(\tau)$ are the Fourier transforms of $\Phi_1(\omega_1)$ and $\Phi_2(\omega_2)$, respectively. This separable state can be understood in terms of statistical independence. The probability of detecting photon 1 *and* photon 2 is $P_1 \cap P_2 = P_1 P_2$, where P_1 and P_2 are the probabilities of detecting photon 1 and photon 2, respectively. In this case, $P_1 = 1 + \Gamma_1(\tau)\cos(\overline{\omega}_1\tau)$ and $P_2 = 1 + \Gamma_2(\tau)\cos(\overline{\omega}_2\tau)$. If $\phi(\omega_1,\omega_2)$ cannot be written as a product of independent functions of ω_1 and ω_2, then the state $|1,1\rangle$ is entangled and $P_{1,2}$ cannot be factored into P_1 and P_2.

The interference pattern of such an entangled two-photon state depends on the particular shape of the joint spectral density. Now, for the case of down-converted photons, we use the initial state given in Eq. (8) to find that

$$P_{1,2}(\tau) \propto \iint d\omega_s d\omega_p \Phi(\omega_s, \omega_p - \omega_s)[1 + \cos(\omega_s\tau)]$$
$$\times [1 + \cos(\omega_p - \omega_s)\tau]. \qquad (16)$$

As discussed in the previous section, we can approximate $\Phi(\omega_s, \omega_p - \omega_s) \approx P(\omega_p)F(\omega_s)$ if $H \approx 1$ in the spectral region defined by the filters. Using this approximation, the integration of Eq. (16) is straightforward and the fourth-order interferogram becomes

$$P_{1,2}(\tau) \propto 1 + \frac{1}{2}\Gamma_p(\tau)\Gamma_F(2\tau) + [\Gamma_p(\tau) + 1]\Gamma_F(\tau)\cos(\omega_0\tau)$$
$$+ \frac{1}{2}\Gamma_p(\tau)\cos(2\omega_0\tau), \qquad (17)$$

where $\Gamma_p(\tau) = \int d\omega_p P(\omega_p + \overline{\omega}_p)\cos(\omega_p\tau)$ and $\Gamma_F(\tau) = \int d\omega_s F(\omega_s + \omega_0)\cos(\omega_s\tau)$. $\overline{\omega}_p$ is the center angular frequency of the pump photons and the filters are selected such that their central frequencies match the center angular frequency of the down-converted photons, that is, $\overline{\omega}_F = \omega_0 = \overline{\omega}_p/2$.

Equation (17) is the main result of this paper. It contains the experimental elements that characterize the complete fourth-order interferogram. The dc term originates from all of the possible distinguishable paths. The second term corresponds to the interference of two identical monochromatic modes. This term is equivalent to the Hong-Ou-Mandel (HOM) effect [17,25]. The third term accounts for the interference of two photons going through different arms [cases iii and iv in Fig. 4(b)]. The last term originates from two photons traveling along the same path [cases i and ii in Fig. 4(b)].

We can extract the envelope functions Γ_p and Γ_F by Fourier transforming Eq. (17). The first two terms, the dc term and $\frac{1}{2}\Gamma_p(\tau)\Gamma_F(2\tau)$, are centered at the zero frequency in the Fourier plane $\widetilde{P}_{1,2}(\varpi)$ of Eq. (17). The third term is centered at $\varpi = \omega_0$ and the fourth term is centered at $\varpi = 2\omega_0$. We can Fourier transform $P_{1,2}(\tau)$ and filter the elements centered at $\varpi = 2\omega_0$ to obtain $\Gamma_p(\tau)$. Then, we can filter the elements around $\varpi = 0$ to obtain $\Gamma_F(\tau)$. With this information, we can estimate the degree of entanglement $\gamma = \Delta\omega_F/\Delta\omega_p$.

IV. EXPERIMENTAL RESULTS

To experimentally confirm Eq. (17), we measured the fourth-order interferogram with two different pairs of filters. Our experiments used a 100 mW diode laser with nominal wavelength of 407 nm and coherence length of 200 μm. The laser pumps a β-barium borate (BBO) nonlinear crystal whose optical axis is oriented at 3.6° with respect to the propagation direction of the laser. This configuration produces type-I, collinearly propagating, down-converted photon pairs with degenerate center wavelengths of 814 nm [29]. After the crystal, the pump laser is suppressed with a combination of a polarizing beam splitter and a longpass filter. The down-converted photons are sent into a Michelson interferometer and the output is analyzed by means of coincidence detection (Fig. 5).

We adjust the path-length difference between the interferometer arms to zero by using a white-light source with a coherence length of 50 μm. The path length of one of the interferometer arms can be adjusted by translating the end mirror with a piezo motor. The latter has a step size of 20 nm. In the experiment, we synchronize the translation of the mirror with the acquisition of photon coincidences. Our coincidence-counting procedure has a time-bin resolution of 4 ps. An electronic delay of 100 ns has been introduced in one of the detection channels in order to shift the center position of the coincidences peak. For all measurements, we used an acquisition time of $T = 10$ seconds and counted all coincidences in a time window $\tau = 3$ ns. Background counts were subtracted using the relation $AB\tau/T$, where A and B are the single-photon counts of detector A and B, and τ and T are the time window and the acquisition time, respectively.

In our theoretical calculations, we assumed that the spectrum of the pump laser is Gaussian with a central wavelength of 407 nm and a FWHM of 0.36 nm, which produces a coherence length $L_p \approx 200$ μm, in agreement with the specifications of the laser. The bandwidth of the down-converted photons is limited by bandpass filters that are placed in front of
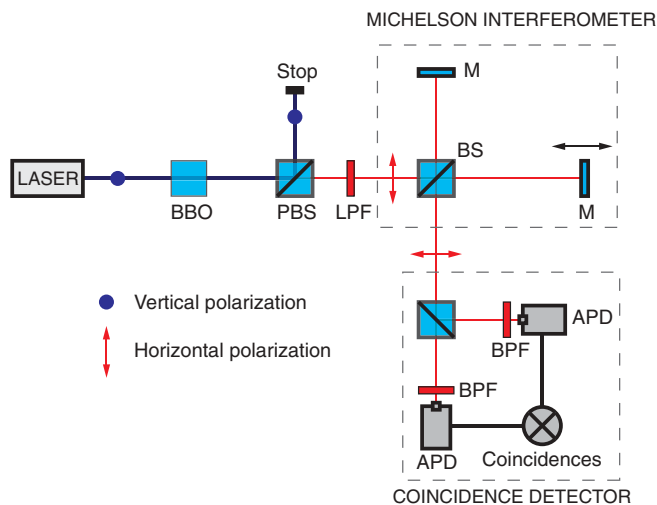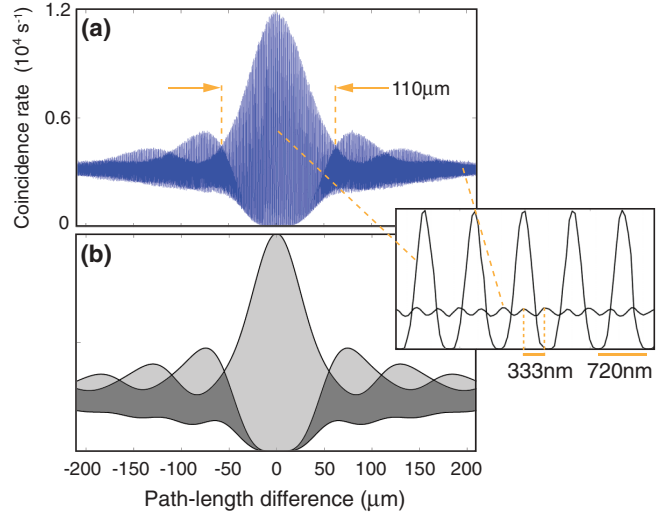

FIG. 6. (Color online) Measurements of the fourth-order interferogram of down-converted photons using 10 nm (FWHM) bandpass filters. The filters produce a coherence length $L_F = 55$ μm. The periodicity of the fringes is 720 and 333 nm when the path-length difference is 0 and 200 μm, respectively. The theoretical calculations are shown in (b). The gray shade represents fringes oscillating at $\lambda_0 = 814$ nm, whereas the dark shade represents fringes oscillating at $\lambda_0/2$. The coherence length of the pump photons is $L_p = 200$ μm.

the detectors. For the first experiment, the filters have a bandwidth of 10 nm centered at 810 nm (the central wavelength is not exactly at the degenerate wavelength of 814 nm; however, because $\Delta\omega_F \gg \Delta\omega_p$, we can still assume that the phase-matching function $H \approx 1$ in the region defined by the filters). For the second experiment, we use bandpass filters with bandwidths of about 200 nm. In this case, the factor γ increases, which is clearly noticeable in the interferogram.

FIG. 5. (Color online) Experimental setup. BBO, β-barium borate crystal; PBS, polarizing beam splitter; LPF, longpass filters; BS, beam splitter; M, mirror; APD, avalanche photodiode; BPF, bandpass filters.
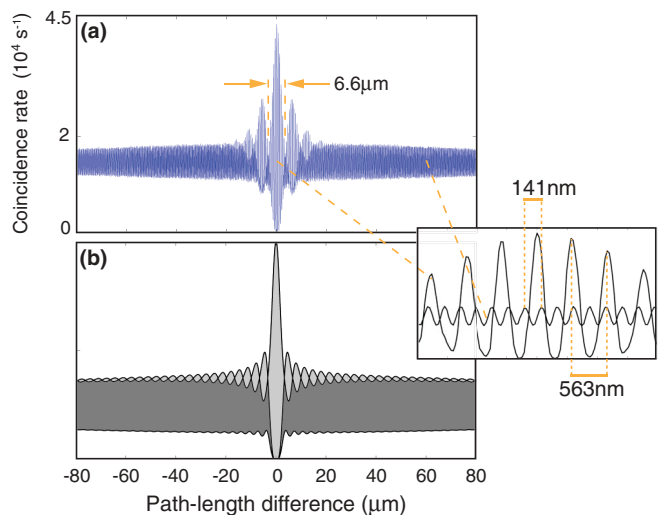

FIG. 7. (Color online) Measurements of the fourth-order interferogram of down-converted photons using 200 nm bandpass filters which produces a coherence length of 3.3 μm. (a) Measurements and (b) theoretical calculations. Compared to the first experiment, the degree of entanglement in the second experiment is higher.

Figure 6(a) shows the measurements of the fourth-order interferogram using the 10 nm filters. The filters give rise to a coherence length of $L_F = 55\ \mu m$. The inset shows a close-up of the fringes in two different regions. In the central region, the oscillations feature a wavelength of 720 nm (visibility of 0.99). On the other hand, for a path-length difference of $200\ \mu m$, the period reduces to 333 nm (visibility of 0.11). The corresponding theoretical calculations based on Eq. (17) are shown in Fig. 6(b). The theory yields an oscillation frequency of ω_0 for short path-length differences (indicated by the gray shade) and $2\omega_0$ for path-length differences larger than the coherence length (indicated by the dark shade). Slight differences between theory and experiment are due to the hysteresis and finite step size of the piezo motor used for mirror translation (the average step size is 20 nm, which generates a path-length difference of 40 nm for each step). Nevertheless, there is good agreement between theory and the experiment.

Figure 7(a) shows the experimental fourth-order interferogram using bandpass filters with a 200 nm bandwidth. The filters produce a coherence length of roughly $L_F = 3.3\ \mu m$. In the central region, the fringes have a period of 563 nm and a visibility of 0.99. When the path-length difference becomes equal to $60\ \mu m$, the wavelength reduces to 141 nm and the visibility reduces to 0.19. The theoretical calculations are shown in Fig. 7(b). The slight frequency mismatch is again due to the precision of the piezo motor. Also, background noise from the pump laser slightly reduces the visibility of the experimentally recorded fringes. Overall, there is good agreement between theory and experiment. Clearly, the degree of entanglement in this experiment is stronger than in the previous one. Since the frequency bandwidth of the filters is increased, the value of γ increases compared to the first experiment (remember that the frequency bandwidth $\Delta\omega_F \propto \Delta\lambda_F$, where $\Delta\lambda_F$ is the wavelength bandwidth). In other words, the area of the joint spectral density selected with the 200 nm bandpass filters is more asymmetric (cf. Fig. 1) than the joint spectral density recorded with 10 nm bandpass filters.

Now that we have demonstrated the validity of Eq. (17), we proceed to characterize the degree of entanglement. We identify three scenarios:

(a) Completely entangled state. This case corresponds to $\gamma \to \infty$, that is, the coherence length L_F of the down-converted photons is $L_F \ll L_p$ [Fig. 8(a)].

(b) Partially entangled state. This is the intermediate case when $L_F \sim L_p$. It corresponds to a superposition of a completely entangled state and a separable state [Fig. 8(b)].

(c) Separable state. In this case, $\gamma \to 0$, which happens when $L_F \gg L_p$ [Fig. 8(c)].

V. CONCLUSIONS AND OUTLOOK

We have analyzed the two-photon Michelson interferometer with entangled down-converted photons. The fourth-order interferogram is given in terms of the pump spectral density and bandwidth of the bandpass filters [Eq. (17)]. We showed that the degree of entanglement increases with the ratio $\gamma = \Delta\omega_F/\Delta\omega_P$, where $\Delta\omega_P$ and $\Delta\omega_F$ are the spectral bandwidths of the pump laser and bandpass filters, respectively. We experimentally measured the complete fourth-order interferogram and the results agree with the theoretical predictions. The second term in Eq. (17) can be used for QOCT [30,31]. The standard implementation of QOCT uses a HOM interferometer [17]. This interferometer uses degenerate, noncollinear, type-I down-converted photons. The down-converted photons enter the two input ports of a beam splitter and the coincidences are detected at the two output ports. The resulting fourth-order interferogram contains a dip at $\tau = 0$. The dip occurs because of the photon bunching effect, which means that the two photons go together to either output ports of the beam splitter.
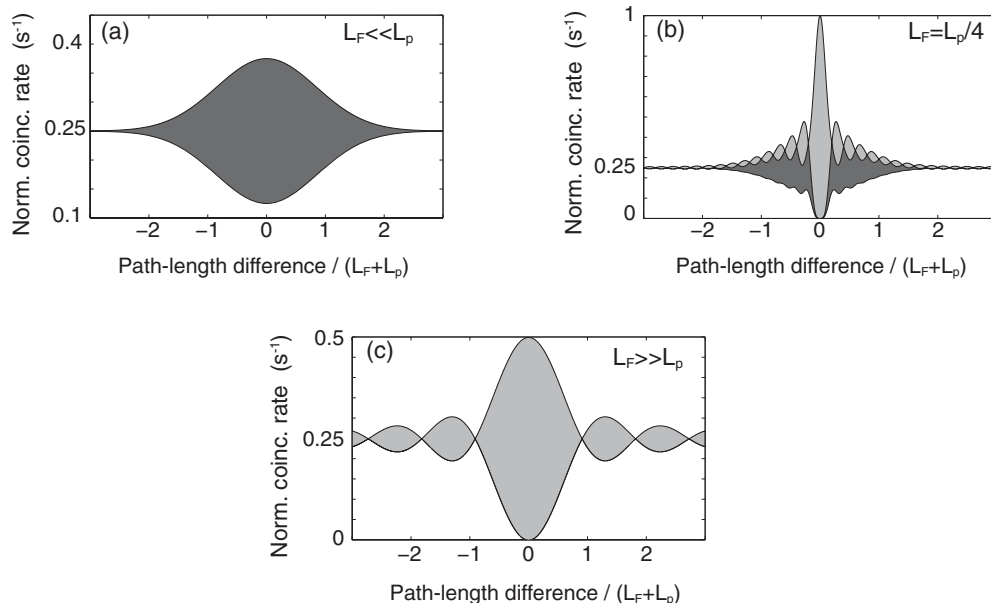

FIG. 8. Interference patterns for different degrees of entanglement. The gray shades indicate fringes with frequency ω_0 and the dark shades indicate fringes with frequency $2\omega_0$. L_p and L_F are the coherence length of the pump and the down-converted photons, respectively. (a) Complete entangled state, (b) partially entangled state, and (c) separable state.

The second term in Eq. (17) is exactly the bunching effect. Therefore, this bunching term presents all of the properties that are required for QOCT, that is, dispersion cancellation and enhancement of resolution by a factor of two. Clearly, from Eq. (17), the bunching term is spectrally separated from the other contributions. We can filter out the other elements by Fourier processing and isolate the bunching term.

[1] A. Einstein, B. Podolsky, and N. Rosen, Phys. Rev. **47**, 777 (1935).

[2] J. S. Bell, Physics **1**, 195 (1964).

[3] S. J. Freedman and J. F. Clauser, Phys. Rev. Lett. **28**, 938 (1972).

[4] A. Aspect, P. Grangier, and G. Roger, Phys. Rev. Lett. **47**, 460 (1981).

[5] E. S. Fry and R. C. Thompson, Phys. Rev. Lett. **37**, 465 (1976).

[6] B. Y. Zel'dovich and D. N. Klyshko, JETP Lett. **9**, 40 (1969).

[7] D. C. Burnham and D. L. Weinberg, Phys. Rev. Lett. **25**, 84 (1970).

[8] D. A. Kleinman, Phys. Rev. **174**, 1027 (1968).

[9] P. G. Kwiat, K. Mattle, H. Weinfurter, A. Zeilinger, A. V. Sergienko, and Y. Shih, Phys. Rev. Lett. **75**, 4337 (1995).

[10] Z. Y. Ou and L. Mandel, Phys. Rev. Lett. **61**, 50 (1988).

[11] J. D. Franson, Phys. Rev. Lett. **62**, 2205 (1989).

[12] M. A. Horne, A. Shimony, and A. Zeilinger, Phys. Rev. Lett. **62**, 2209 (1989).

[13] L. Mandel, Rev. Mod. Phys. **71**, S274 (1999).

[14] M. Teich, B. Saleh, F. Wong, and J. Shapiro, Quantum Inf. Proc. **10**, 1 (2011).

[15] A. N. Boto, P. Kok, D. S. Abrams, S. L. Braunstein, C. P. Williams, and J. P. Dowling, Phys. Rev. Lett. **85**, 2733 (2000).

[16] L. A. Lugiato, A. Gatti, and E. Brambilla, J. Opt. B **4**, S176 (2002).

[17] C. K. Hong, Z. Y. Ou, and L. Mandel, Phys. Rev. Lett. **59**, 2044 (1987).

[18] Z. Y. Ou, X. Y. Zou, L. J. Wang, and L. Mandel, Phys. Rev. A **42**, 2957 (1990).

[19] Y. H. Shih, A. V. Sergienko, and M. H. Rubin, Phys. Rev. A **47**, 1288 (1993).

[20] J. Brendel, E. Mohler, and W. Martienssen, Phys. Rev. Lett. **66**, 1142 (1991).

[21] P. G. Kwiat, W. A. Vareka, C. K. Hong, H. Nathel, and R. Y. Chiao, Phys. Rev. A **41**, 2910 (1990).

[22] J. G. Rarity, P. R. Tapster, E. Jakeman, T. Larchuk, R. A. Campos, M. C. Teich, and B. E. A. Saleh, Phys. Rev. Lett. **65**, 1348 (1990).

[23] P. G. Kwiat, A. M. Steinberg, and R. Y. Chiao, Phys. Rev. A **47**, 2472(R) (1993).

[24] E. J. Galvez, C. H. Holbrow, M. J. Pysher, J. W. Martin, N. Courtemanche, L. Heilig, and J. Spencer, Am. J. Phys. **73**, 127 (2005).

[25] S. Odate, H.-B. Wang, and T. Kobayashi, Phys. Rev. A **72**, 063812 (2005).

[26] B. J. Smith and M. G. Raymer, New J. Phys. **9**, 414 (2007).

[27] P. G. Kwiat, J. Mod. Opt. **44**, 2173 (1997).

[28] Z. Y. J. Ou, *Multi-photon Quantum Interference* (Springer, New York, 2007).

[29] N. Boeuf, D. Branning, I. Chaperot, E. Dauler, S. Guérin, G. Jaeger, A. Muller, and A. Migdall, Opt. Eng. **39**, 1016 (2000).

[30] A. F. Abouraddy, M. B. Nasr, B. E. A. Saleh, A. V. Sergienko, and M. C. Teich, Phys. Rev. A **65**, 053817 (2002).

[31] M. B. Nasr, B. E. A. Saleh, A. V. Sergienko, and M. C. Teich, Phys. Rev. Lett. **91**, 083601 (2003).